KSME Journal, Vol. 7, No. 3, pp. 203~212, 1993

Numerical Computation for Heat Transfer in Crystal Growth

Hiroyuki Ozoe*

(*Received August 10, 1992*)

The numerical analyses for crystallization processes are selected and summarized from the author's recent works. The importance of heat transfer may be noted in the phase change manufacturing processes from liquid to solid. The effect of convection on the curved interface may be also noted in the floating zone crystallization process. Specifically, the processes presented are as follows. Three-dimensional cylindrical coordinate model for a Czochralski bulk flow of liquid metal in a horizontal or a vertical magnetic field is presented and numerically solved for selected conditions. Then, a floating zone crystallization method is modeled by an axisymmetric coordinate and then solved by an isoparametric finite element method for curved solid/melt interfaces and a gas/melt interface. Sample computational results are also presented.

Key Words: Crystal Growth, Czochralski Flow, Heat Transfer, Magnetic Force, Material Processing

Nomenclature

B_0 : Bond number $=\Delta\rho g r_0^2/\sigma$ = Buoyancy force /Surface tension force

Bi^* : Biot number $=h_{eq} r_0/k$ = convective heat transfer rate/conductive rate

b : Magnetic induction vector, kg $s^{-2}A^{-1}$

C : Dimensionless concentration

C_p : Specific heat, J/kg K

e : Electric field, m kg $s^{-3}A^{-1}$

f : Lorentz force, N m^{-3}

Gr^* : Modified Grashof number $=g\beta r_0^5 q/(k\nu^2)$ = buoyancy force/inertial force

g : Acceleration due to gravity, m/s^2

H : Dimensionless height of a crucible

Ha : Hartmannumber $=\sqrt{\sigma_e/\mu}\, B_0 h$ = Lorentz force/viscous force

h : Height of a crucible, m

h_{eq} : Equivalent heat transfer coefficient, J/m^2Ks

j : Electric current density, Am^{-3}

k : Thermal conductivity, J/msK

ls : Radius of a crystal rod, m

Ma : Marangoni number $=(C_p r_0^3 q/\nu k^2)(-\partial\sigma/\partial\theta)$ = surface tension force/viscous force

Nu : Nusselt number

P : Lagrange multiplier $=\Delta p r_0/\sigma$

Δp : Dimensionless Lagrange multiplier, N/m^2

Pr : Prandtl number $=\nu/\alpha$

q : rate of heat generation, J/m^3s

R : Dimensionless radius $=r/r_0$

Ra : Rayleigh number $=Gr \cdot Pr$

Re : Reynolds number $=l_s^2\omega/\nu$

r : Radial coordinate, m

r_0 : Radius of a rod, m

t : Time, s

t_0 : r_0^2/α, s

T : Dimensionless temperature $=(\theta-\theta_m)/\theta_a$

T_w : Dimensionless wall temperature

T_∞ : Dimensionless ambient temperature

U : Dimensionless radial velocity $=u/u_0$

u : Radial velocity, m/s

u_0 : α/r_0, m/s

v : Velocity component in the circumferential direction

V : Dimensionless velocity component in the circumferential direction $=v/u_0$

V : Velocity vector, m/s

W : Dimensionless axial velocity $=w/u_0$

w : Axial velocity component, m/s

* Institute of Advanced Material Study, Kyushu University, Japan

Z : Dimensionless axial coordinate $= z/r_0$
z : Axial coordinate, m

Greek letters

α : Thermal diffusivity, m^2/s
β : Volumetric coefficient of expansion, 1/K
$\Delta\rho$: Density difference between gas and liquid, kg/m^3
θ : Temperature, K
θ_a : Reference temperature [K]
θ_m : Melting temperature, K
θ_w : Wall temperature, K
θ_∞ : Ambient temperature, K
μ : Viscosity, kg/ms
ν : Kinematic viscosity, m^2/s
ρ : Density, kg/m^3
σ : Surface tension, N/m
τ : Dimensionless time $= t/t_0$
λ : Thermal conductivity, $Wm^{-1}K^{-1}$
ω : Angular velocity of a crystal rod, rad s^{-1}
ϕ : Circumferential coordinate, rad
ϕ_f : Contact angle, rad
Ψ : Dimensionless stream function $= \psi/\alpha$, -
ψ : Stream function, m^2/s
Ω : Dimensionless vorticity $= \zeta r_0^2/\alpha$
ζ : Vorticity, 1/s
σ_e : electric conductivity, $m^{-3}kg^{-1}\ s^3\ A^2$

Subscript

0 : Reference value for a dimensionless variable
c : Cold wall
h : Hot wall

Superscript

T : Transpose of the vector

Operator

∇ : $[\partial(r)/r\partial r,\ \partial/r\partial\phi,\ \partial/\partial z]$ (dimensional or dimensionless)
∇^2 : $\partial^2/\partial R^2+(\partial/\partial R)/R+\partial^2/R^2\partial\phi^2+\partial^2/\partial Z^2$
$D/D\tau$: $\partial/\partial t+U\partial/\partial R+V\partial/R\partial\phi+W\partial/\partial Z$

1. Introduction

This is a research summary of our current works on numerical heat transfer in crystal growth. The purpose of this paper is to present the numerical computations of crystal growth and to emphasize the importance of the heat transfer in material processing. In crystal growth, the feed material is once heated to liquid state and then mono crystal solid is grown up epitaxially starting from a small piece of monocrystal seed. In this process, conductive and radiative cooling works in a phase change process from liquid to solid. The convection also plays an intrinsic effect on the quality of monocrystal rod especially on its impurity distribution. The monocrystal rod is then sliced to many pieces of crystal wafers to serve as substrates for electric integrated circuits.

The electrical integrated circuits are mounted on a crystal substrate prepared from a crystal rod such as silicon and gallium arsenide whose purity affects the critical function of semiconducting characteristics. Most of the current silicon rods are manufactured with a pulling-up Czochralski method from molten silicon kept in a SiO_2 crucible. In this process, oxygen molecules are dissolved from a crucible wall into molten silicon and convected to a crystal rod and then included in a crystal rod as impurities. To control the amount of oxygen molecules, an application of an external magnetic field has been found to be effective. However, the direction and strengths etc. of the magnetic field appear to be applied on a trial and error basis.

The application of an external magnetic field in a solidification process of alloys was tried by Abe et al.(1962). Then, Utech and Fleming(1966) also employed a vertical magnetic field in a floating boat solidification process of Indium antimonide and reported drastic decrease of temperature fluctuation in molten liquid. Witt et al.(1970) employed a lateral magnetic field in a Czochralski crystallization process of Indium antimonide and reported effectiveness of a magnetic field. Numerical analysis of this process has been reported by Langlois(1982), Mihelcic(1984) Walker and Hjelming(1986), and Brown et al(1988).

This paper aims to present numerical computations to clarify the transport phenomena in the bulk convection of melt and phase change processes and to emphasize the importance of the heat transfer in material processing. This paper also tries to invite the heat transfer people to the field of material processing because heat transfer is one

of the critical mechanism in many processes of material manufacturing.

2. Czochralski Bulk Flow in a Horizontal Magnetic Field(Toh and Ozoe, 1992)

2.1 Model equations and boundary conditions

Schematics of the Czochralski crystallization is shown in Fig. 1. A crystal rod is manufactured by radiation cooling from the surface of the melt of feed material.

The modeled system for the Czochralski melt convection system is shown in Fig. 2. Melt is filled in a cylindrical crucible and a model for a crystal rod is rotating on the liquid surface. The crucible is heated from surroundings and a crystal rod is cooled from ambient environment. Because of the rotational crystal rod, the melt flow may be presumed to be axisymmetric. However, under a horizontal lateral magnetic field, the field analysis requires a fully three-dimensional model.

The basic equations for convection of liquid metal in a crucible under a lateral magnetic field consists of a continuity equation for material, an energy equation, three momentum equations in radial, circumferential and vertical directions, and the continuity equation for an electric current. The Boussinesq approximation was employed that the physical properties are constant except that of density in a buoyant term. Then, after nondimensionalization these equations become as follows;

$$\nabla \cdot V = 0, \tag{1}$$

$$DT/D\tau = \nabla^2 T, \tag{2}$$

$$DV/D\tau = Pr\nabla^2 V - \nabla \cdot P - PrT(0, 0, 1)^T - Ha^2 Ra^{-2/3} PrF + (V^2/R, -UV/R, 0)^T + 2Pr(-\partial V/R^2\partial\phi, \partial U/R^2\partial\phi, 0)^T, \tag{3}$$

$$\nabla^2 \Psi = \nabla \cdot (V \times B) \tag{4}$$

The dimensionless variables are defined as follows.

$$R = r/r_0,\ Z = z/r_0,\ U = u/u_0,\ V = v/u_0,$$
$$W = w/u_0,\ T = (\theta - \theta_0)/(\theta_h - \theta_c),\ P = p/p_0,$$
$$\Psi = \psi/\psi_0,\ \tau = t/t_0,\ r_0 = [g\beta(\theta_h - \theta_c)/\alpha\nu]^{-1/3},$$
$$u_0 = \alpha/r_0,\ p_0 = \rho u_0^2,\ t_0 = r_0^2/\alpha,\ \psi_0 = B_0\alpha,$$
$$\theta_0 = (\theta_h + \theta_c)/2,\ \omega_0 = \alpha/r_0^2,\ Pr = \nu/\alpha,$$
$$Ha = (\sigma_e/\mu)^{1/2} B_0 h,\ Ra = g\beta(\theta_h - \theta_c)h^3/\alpha\nu,$$
$$Re = ls^2\omega/\nu,\ F = fr_0/\sigma_e B_0^2 \alpha,\ B = b/B_0$$

For the liquid metal, an electric neutrality was assumed and the Lorentz force can be expressed as follows (Ozoe and Toh, 1990).

$$f = j \times b = \sigma_e(-\nabla\psi + v \times b) \times b, \tag{5}$$

where j represents electric current and b magnetic induction for which a uniform horizontal component was assumed. For electric field, electric

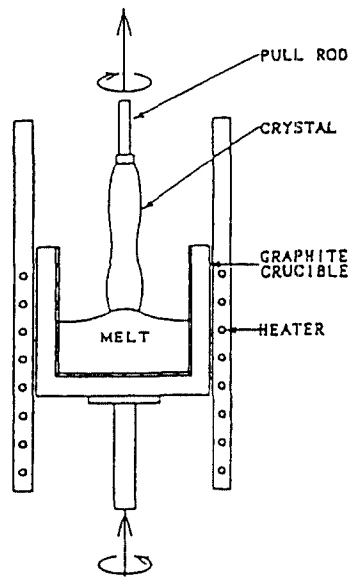

Fig. 1 Czochralski method

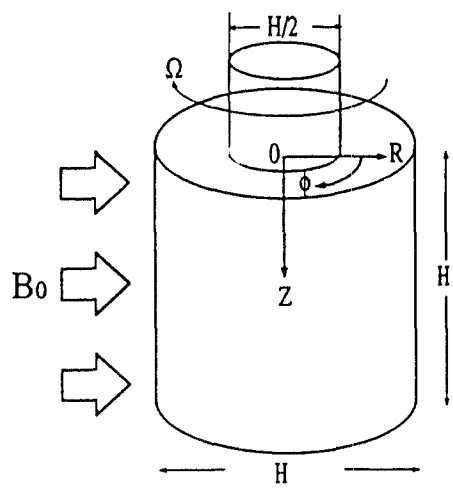

Fig. 2 Model geometry for a lateral magnetic field

scalar potential ψ was asumed following S. Kobayashi(1986). The electric scalar potential was solved under continuity condition for electric current j as follows.

$$\nabla \cdot j = \sigma\varepsilon(-\nabla^2 \psi + \nabla \cdot (v \times b)) = 0 \tag{6}$$

The horizontal magnetic induction B_0 is divided in a radial and a circumferential direction as follows.

$$b = \begin{pmatrix} b_r \\ b_\phi \\ b_z \end{pmatrix} = \begin{pmatrix} B_0 \cos\phi \\ -B_0 \sin\phi \\ 0 \end{pmatrix} \tag{7}$$

The boundary conditions are as follows.

$$T = 0.5,\ U = V = W = 0,\ \partial\Psi/\partial R = 0 \quad \text{at } R = H/2 \tag{8}$$

$$T = 0.5,\ U = V = W = 0,\ \partial\Psi/\partial Z = 0 \quad \text{at } Z = H \tag{9}$$

At $Z=0$ and $0 \leq R \leq H/4$, the solidifying interface between liquid and a rotating crystal rod was assumed to be flat and kept at a colder uniform temperature. Then,

$$T = -0.5,\ U = W = 0,$$
$$V = R\Omega = R(16\ Pr\ Re\ Ra^{-2/3}),$$
$$\partial\Psi/\partial Z = -(U\sin\phi + V\cos\phi) \tag{10}$$

The boundary condition for an electric scalar potential is to represent no electric current through the interface at $Z=0$.

At $Z=0$ and $H/4 \leq R \leq H/2$, the gas-liquid interface is thermally insulated and free-slip and no electric current was assumed as follows.

$$\partial T/\partial Z = 0,\ W = 0,\ \partial U/\partial Z = \partial V/\partial Z = 0,$$
$$\partial\Psi/\partial Z = -(U\sin\phi + V\cos\phi) \tag{11}$$

2.2 Numerical scheme

The computational domain expressed in a cylindrical coordinate system was divided into control volumes and HSMAC method(1972) was employed. The grid allocation in a vertical cross section of a cylinder is shown in Fig. 3. Half grid is taken over a center line to satisfy the continuity of physical properties. The values at the first half grid supply the boundary conditions for the computation in another half vertical plane.

2.3 Computed results

At the beginning, numerical computaion was carried out for the non-magnetic field. Computing

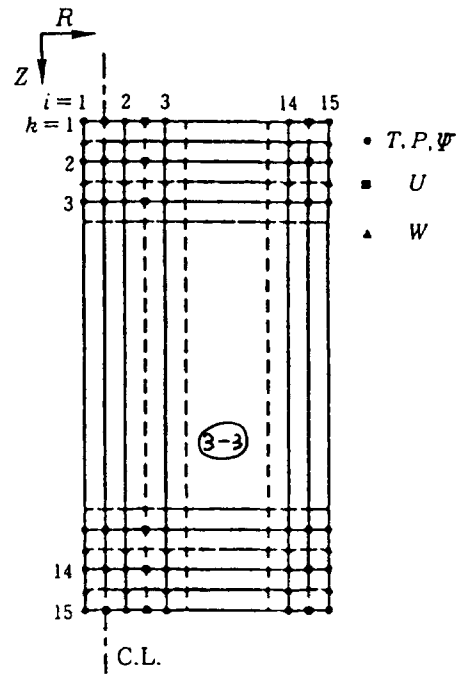

Fig. 3 Vertical cross section of grid points

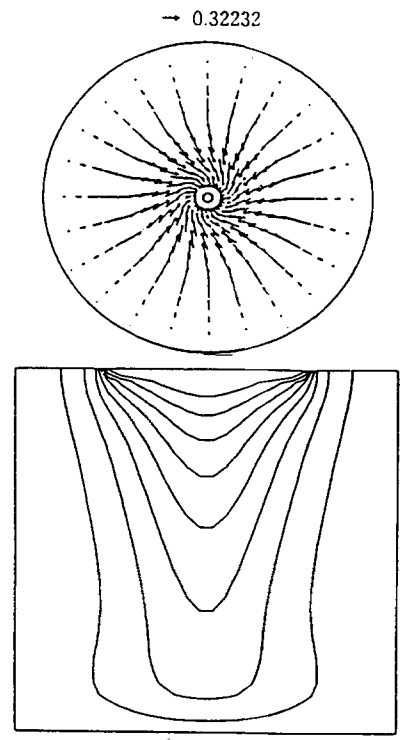

Fig. 4 Converged solutions without an external magnetic field : Ha=0, Pr=0.01, Ra=10^7 and Re=1620

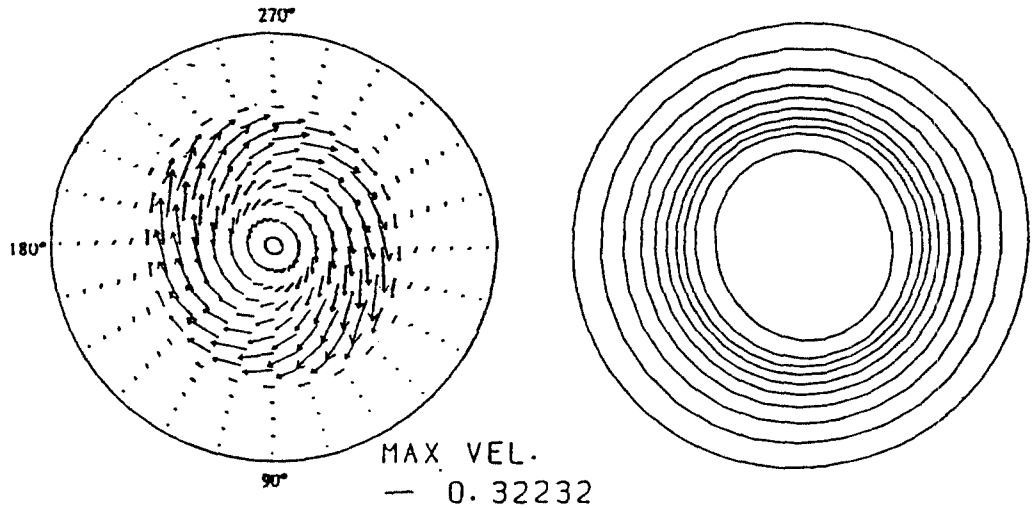

Fig. 5 Converged solutions in a lateral magnetic field : Ha=100, Pr=0.01, Ra=105 and Re=1620

condition is $Gr=10^7$, $Pr=10^{-2}$, $Re=1620$ and $Ha=0$. The converged velocity vectors in a horizontal cross section at $Z=0.038H$ and isotherms in a vertical cross section are shown in Fig. 4. Both velocity vectors and isotherms are axially symmetric which support somewhat the reliability of the present computaion. In a horizontal magnetic field at $Ha=100$, the horizontal velocity vectors and isotherms become as shown in Fig. 5(a) and (b). These suggest non-axisymmetric velocity and isothermal profiles to support fully three-dimensional numerical analysis even with a rotating top crystal rod.

3. Czochralski Bulk Flow in an Axial Magnetic Field(Ozoe and Toh, 1990)

An axial magnetic field has been also employed and an axial symmetry may be assumed for this system. The modeled area is shown in Fig. 6. The model equations can be simplified to delete the gradient in a circumferential direction ϕ. Computed isotherms and velocity vectors at $Gr/Re^2=4$, $Pr=0.054$, and $Gr=10^6$ are shown in Fig. 7. The average radial velocity decreased from 0.09 at $Ha=0$ to 0.003 at $Ha=1000$ but the average circumferential velocity decreased to 0.0215 from 0.548. The average Nusselt number at a phase-change interface of a rotating crystal rod decreased from 1.14 at $Ha=0$ to 1.037 at $Ha=1000$. In any cases, the velocity and heat flux decreased extensively.

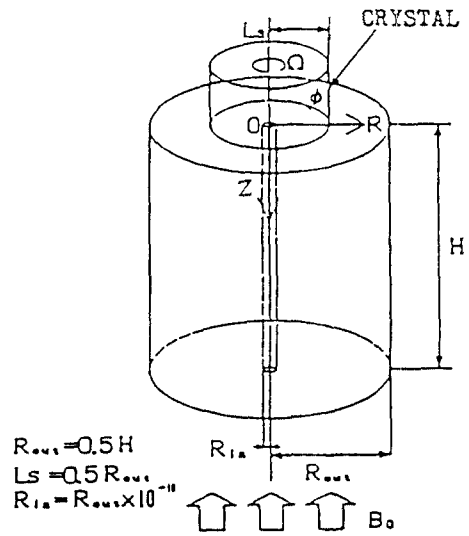

Fig. 6 Model geometry for an axial magnetic field

4. Floating Zone Crystallization

(Ozoe and Tanaka, 1991; Imai and Ozoe, 1992)

A floating zone crystallization method melts a feed rod locally by a radio frequency coil and the melted material is just kept by a surface tension

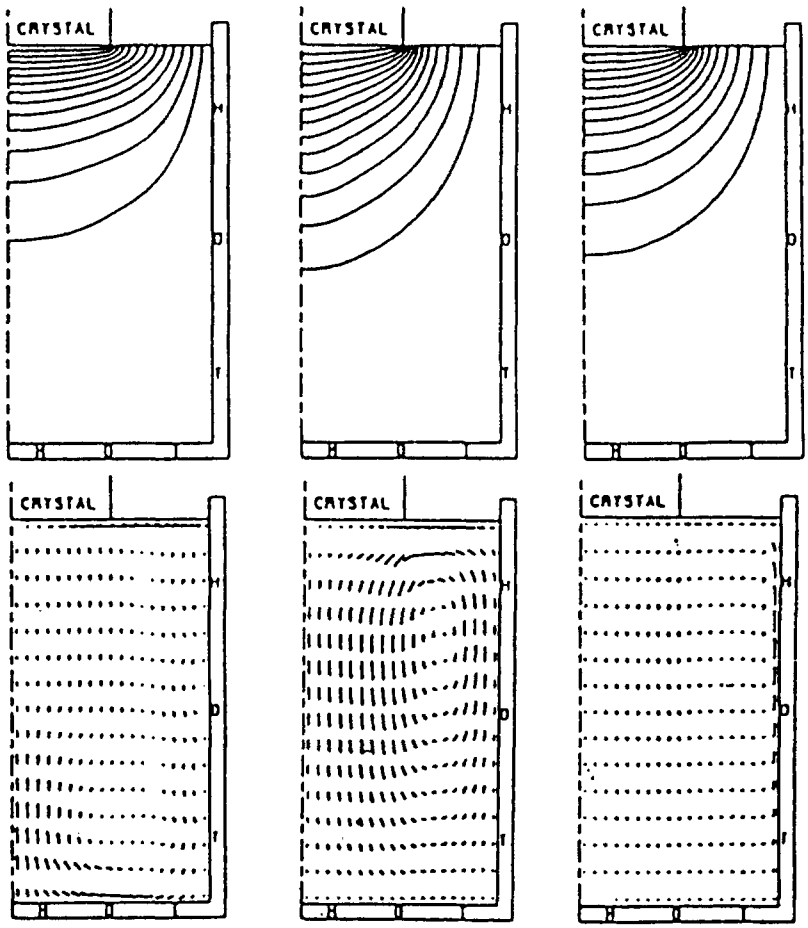

Fig. 7 Computed isotherms and velocity vectors at $Gr/Re^2=4.0$, $Gr=10^6$, $Pr=0.054$ and $Re=500$ Isotherms are every 1/15 between the maximum temperature at a crucible wall and the minimum at a crystal bottom

force between a feed rod and a crystal rod. This scheme has no vessel and no contamination. There are many papers to have analyzed this process. Some of them are by Duranceau and Brown(1986), Smith(1986) and others. However, the detailed computational scheme is not clear and the development of a numerical scheme is required for more detailed analyses including the effects of gravity, rotation and magnetic field, etc.

A finite element computational scheme was developed to get a curved solid-liquid interface between a feed rod, melt and a single crystal rod. The simplification for a straight surface between a melted layer and surrounding gas was studied in a first step and then a curved surface was also included for simulation.

4.1 Model equations and boundary conditions

Schematic view of the floating zone crystallization is shown in Fig. 8. The model for this is shown in Fig. 9. The aspect ratio of a cylinder rod is three, i. e., the length of a radius is unity and that of an axis is 3. The region from $Z=1.24$ to 1. 76 was assumed to generate heat uniformly. The basic equations consist of a continuity equation, and energy equation for both a solid and a melted regime, momentum equations for melted regime and a state equation for liquid. After introducing a Boussinesq assumption, partial derivatives of two momentum equations were taken to delete pressure terms by subtracting each other to give a

vorticity equation. A stream function was introduce to satisfy the equation of continuity. The nondimensionalized system equations are finally obtained as follows.

$$\frac{DT}{D\tau}=\nabla^2 T+1, \tag{12}$$

$$\frac{D\Omega}{D\tau}-\frac{U\Omega}{R}=Pr\left(\nabla^2\Omega-\frac{\Omega}{R^2}\right)+Gr^*Pr^2\frac{\partial T}{\partial R}, \tag{13}$$

$$U=-\frac{\partial\Psi}{\partial Z}, \tag{14}$$

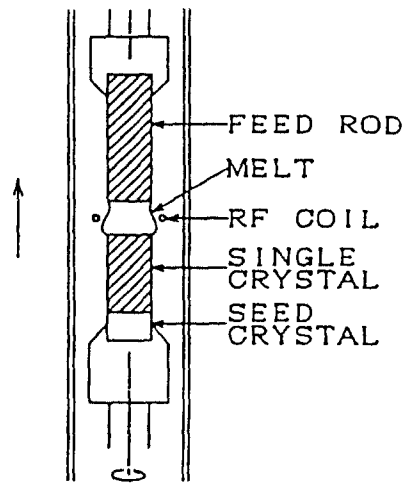

Fig. 8 Schematic of a Fz crystallization method

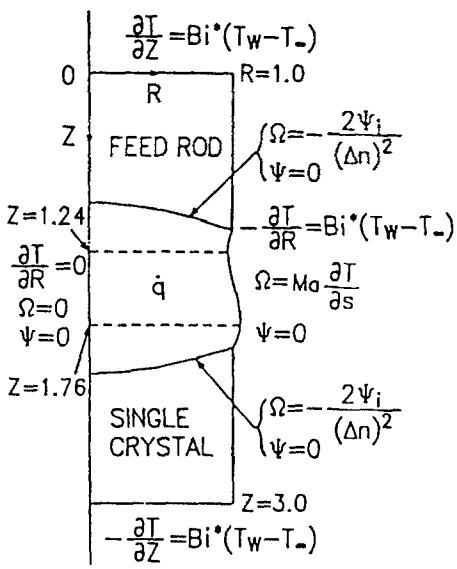

Fig. 9 Boundary conditions for a Fz model

$$W=\partial(R\Psi)/R\partial R, \tag{15}$$

$$\Omega=-\nabla^2\Psi+\frac{\Psi}{R^2} \tag{16}$$

The dimensionless variables are defined as follows.

$$\begin{aligned}&R=r/r_0,\ Z=z/z_0,\ U=u/u_0,\ W=w/u_0,\\&T=(\theta-\theta_m)/\theta_a,\ \tau=t/t_0,\ u_0=\alpha/r_0,\\&\theta_a=qr_0^2/k,\ Pr=\nu/\alpha,\ t_0=r_0^2/\alpha,\\&Gr^*=g\beta r_0^5 q(k\nu^2),\ Bi^*=h_{eq}r_0/k,\\&Ma=(C_p r_0^3 q/\nu k^2)(-\partial\sigma/\partial\theta),\\&h_{eq}=h+\varepsilon\sigma F(\theta_w^2+\theta_\infty^2)(\theta_w+\theta_\infty),\\&Pe=r_0^2\omega/\alpha\end{aligned} \tag{17}$$

The equivalent heat transfer coefficient includes both the convective and the radiative heat transfer effect. The boundary conditions are all listed in Fig. 9. The rate of heat generation q was presumed to be uniform between two hatched lines. According to Coriell and Cordes(1977), the curved surface can be computed by solving the following simultaneous equations. These are based on the well-known Laplace-Yang capillary equations.

$$\frac{\partial R}{\partial S}=\sin\phi,\ \frac{\partial Z}{\partial S}=\cos\phi \text{ and}$$

$$\frac{\partial\phi}{\partial S}=\frac{\cos\phi}{R}+B_0Z-P-\varepsilon_r V^2, \tag{18}$$

where

$$B_0=\Delta\rho g r_0 2/\sigma \text{ and } P=\Delta P_0/\sigma \tag{19}$$

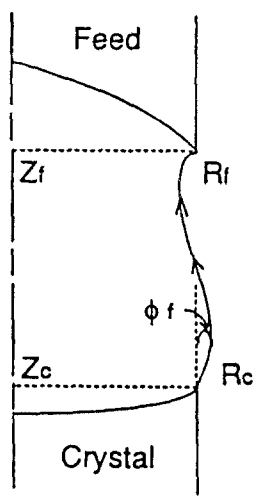

Fig. 10 Boundary conditions for Laplace-Yang Capillary equations

The Runge-Kutta integration was employed to solve the above simultaneous equations with the starting angle ϕ_f at $Z=Z_c$ as shown in Fig. 10. Changing the Lagrange parameter P, the free surface was determined to get to (R_f, Z_f).

4.2 Computed results

Presuming there is no Marangoni convection, the gravitational force gives convection as shown in Fig. 11 for velocity vectors, stream function, isotherms and FEM grids for $Gr^*=10^4$, $Pr=0.01$, $T_\infty=-2.02$, $Bi^*=0.037$, $B_0=1.25$, $P=2.22$, $\varepsilon_r=6\times10^{-5}$, $\phi_f=0.5$, $Pe_1=Pe_2=0$. When both the upper rod (feed) and the lower rod (crystal) are rotated in a reverse direction, then we get those as shown in Fig. 12. Because of the centrifugal force, a single roll cell is separated to double cell in a donut shape. The circumferential velocity becomes zero between two roll cells as shown in picture (d).

When the surface tension (Marangoni) force is

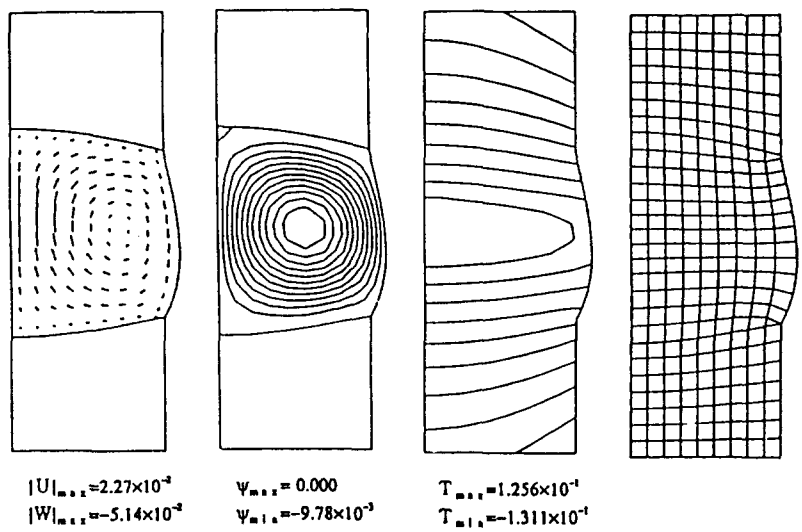

Fig. 11 Converged solutions at Non-Marangoni condition : $Gr^*=10000$, $Pr=0.01$, $T_\infty=-2.02$, $Bi^*=0.037$, $B_0=1.25$, $\varepsilon_r=6\times10^{-5}$, $\phi_f=0.5$, $Pe_1=0.0$ and $Pe_2=0.0$. Isotherms are every 1/10 between $T_{max}=0.1256$ and $T_{min}=-0.1311$. This is also the case for Figs. 12 and 13.

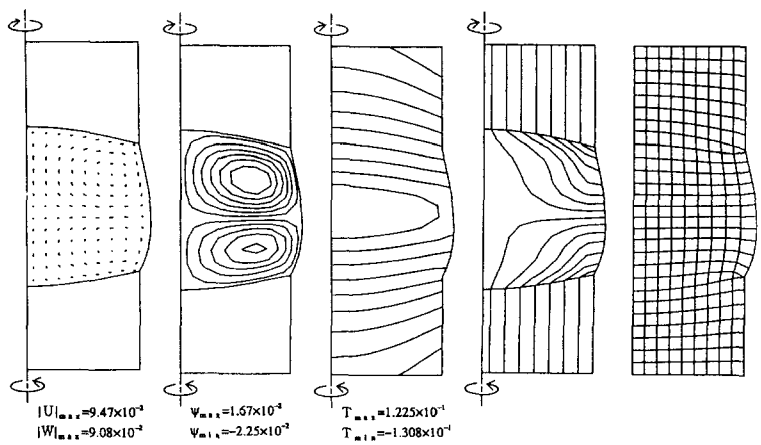

Fig. 12 Converged solutions at $Pe_1=1.0$ and $Pe_2=-1.0$. Other conditions are the same as those of Fig. 11.

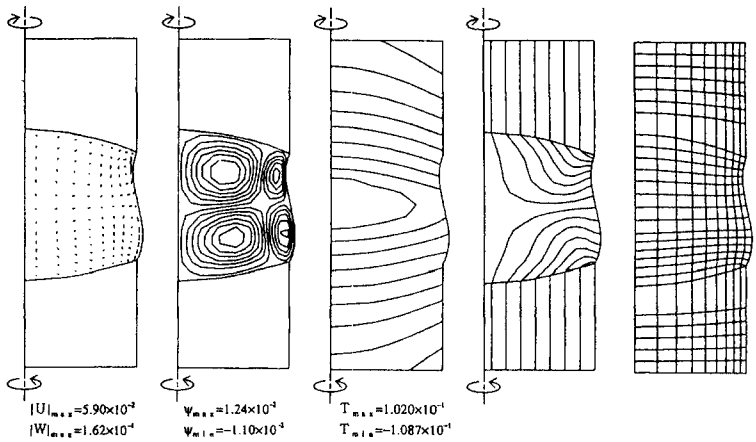

Fig. 13 Converged solutions at $Pe_1=1.0$ and $Pe_2=-1.0$. $Ma=25$, $Gr^*=100$, $Pr=0.01$, $T_\infty=-1.518$, $Bi^*=0.037$, $B_0=5$, $\varepsilon_r=3\times10^{-5}$, $\phi_f=0.5$ and $P=3.58$.

included, the situation becomes more complicated. One of the result is shown in Fig. 13. The conditions are $Ma=25$, $Gr^*=100$, $Pr=0.01$, $T_\infty=-1.518$, $Bi^*=0.037$, $B_0=5$, $\varepsilon_r=3\times10^{-5}$, $\phi_f=0.5$, $P=3.58$, $Pe_1=1$, $Pe_2=-1$. Centrifugal force gives large internal roll cells and the surface tension force gives smaller roll cells near the curved surface.

5. Concluding Remarks

Various material processes including crystal growth as described above are critically affected by heat transfer. Better design and control for these processes would lead us to a better and more efficient way of manufacturing materials. For this purpose the corresponding transport processes should be clarified. The present simulation is only at a preliminary stage for this and is required to be refined in future.

Acknowledgement

Present author appreciate very much for the opportunity to publish this article in this Journal with the invitation by an associate editor, Professor Jae-Heon Lee. This article is some of the recent research work conducted by the author's research group and is an extended part of the works presented at the seminars at Hanyang University, KIST and KAITEC in September, 1991. Support from KOSEF is acknowledged very much.

References

Abe, T. et al., 1962, "A Monthly Publication of the Japan Society of Applied Physics," Vol. 31, pp. 58.

Brown, R.A., 1988, "Theory of Transport Processes in Single Crystal," AIChE Journal, Vol. 34, pp. 881~911.

Coriell, S.R. and Cordes, M. R., 1977, "Theory of Molten Zone Shape and Stability," J. Crystal Growth, Vol. 42, pp. 466~472.

Duranceau, J.L. and Brown, R.A., 1986, "Thermal Capillary Analysis of Small-Scale Floating Zones ; Steady State Calculations," J. Crystal Growth, Vol. 75, pp. 367~389.

Hirt, C.W. and Cook, J.L., 1972, "Calculating Three-Dimensional Flows around Structures and over Rough Terrain," Journal Computational Physics, Vol. 10, pp. 324~340.

Hjelming, L.N. and Walker, J.S., 1986, "Melt Motion in a Czochralski Crystal Puller with an Axial Magnetic Field : Isothermal Motion," Journal of the Fluid Mechanics, Vol. 164, pp. 237~273.

Imai, K. and Ozoe, H., 1992, "Numerical Computation of Fz Crystallization with Internal He-

at Generation," Kagaku Kogaku Saga Meeting.

Kobayashi, S., 1986, "Effect of an Axial Magnetic Field on Solute Distribution in Czochralski Grown Crystals-a Theoretical Analysis," Journal of Crystal Growth, Vol. 75, pp. 301～308.

Langlois, W.E., 1982, "A Parameter Sensitivity Study for Czochralski Bulk Flow Silicon," Journal of Crystal Growth, Vol. 56, pp. 15～18.

Mihelcic, M., Wingerath, K. and Pirron, C., 1984, "Three-Dimensional Simulations of the Czochralski Bulk Flow," Journal of Crystal Growth, Vol. 69, pp. 473～488.

Ozoe, H. and Toh, K., 1990, "Numerical Computation for a Czochralski Bulk Flow of Liquid Metals under a Vertical External Magnetic Field," The 9th International Heat Transfer Conference, Jerusalem, Vol. 6, pp. 311～316.

Ozoe, H. and Tanaka, S., 1991, "Finite Element Analyses of a Simplified Model for Floating Zone Crystallization Method," Proc. of the 4th International Symposium on Transport Phenomena in Heat and Mass Transfer, Sydney.

Smith, M.K., 1986, "Thermocapillary and Centrifugal-Buoyancy-Driven Motion in a Rapidly Rotating Liquid Cylinder," J. Fluid Mech., Vol. 166, pp. 245～264.

Toh, K. and Ozoe, H., 1992, "Three-Dimensional Czochralski Flow of Liquid Metal in a Lateral Magnetic Field." 1st International Conference on Transport Phenomena in Processing, Hawaii.

Utech, U.P. and Fleming, M.C., 1966, "Elimination of Solute Banding in Indium Antimonide Crystals by Grown in a Magnetic Field," Journal of Applied Physics, Vol. 37, pp. 2021～2024.

Witt, A. F., Hertman, C.J. and Gatos, H.C., 1970, "Czochralski-Type Crystal Growth in Transverse Magnetic Fields, The Observation of Magnetic Domain Structures of the Intermetallic Compounds $SnCo_5$, $LaCo_5$ and $CeCo_5$," Journal of Materials Science, Vol. 37, pp. 822～824.